

---

# Approximate Bayesian inference in spatial environments

---

Atanas Mirchev

Baris Kayalibay

Patrick van der Smagt

Justin Bayer

Data:Lab, Volkswagen Group  
{firstname.lastname}@volkswagen.de

## Abstract

We propose to learn a stochastic recurrent model to solve the problem of simultaneous localisation and mapping (SLAM). Our model is a deep variational Bayes filter augmented with a latent global variable—similar to an external memory component—representing the spatially structured environment. Reasoning about the pose of an agent and the map of the environment is then naturally expressed as posterior inference in the resulting generative model. We evaluate the method on a set of randomly generated mazes which are traversed by an agent equipped with laser range finders. Path integration based on an accurate motion model is consistently outperformed, and most importantly, drift practically eliminated. Our approach inherits favourable properties from neural networks, such as differentiability, flexibility and the ability to train components either in isolation or end-to-end.

## 1 Introduction

Sequential decision making is a framework to represent the interaction of an agent with its environment: an observation of the world is presented to the agent, upon which the agent picks an action, which in turn alters the world’s state. The agent then observes the new state of the world, and the process repeats. In the case of mobile agents, the state of the world includes the location of the agent. Knowing that location, or at least having an accurate estimate of it, is crucial for devising and successfully executing plans.

One obvious way of estimating an agent’s location is that of *odometry* or *path integration*: an approximate motion model is used to get an estimate of the change in location at each time step, which is summed up to give an overall estimate. But such estimates are rarely without error, and since even tiny errors accumulate over time the result deteriorates and is ultimately useless. Alternatively, one can estimate the current location based on the current observation. This approach often suffers from perceptual aliasing, where multiple positions share the same sensor readings. The problem gets aggravated when a map is not available and has to be estimated online (cf. fig. 1).

The robotics community has developed a range of methods to solve that problem under the umbrella term of simultaneous localisation and mapping (SLAM). The current de facto standard formulation is based on combining the imperfect estimates stemming from the map and the motion model to obtain a better, combined estimate. This is conceptually easy in a probabilistic framework: the beliefs are “fused” according to Bayes’ theorem. The resulting model, a Bayes filter, lies at the heart of

---

PvdS and JB conceived the project. JB lead the project. AM, BK and JB devised the method. AM implemented the method with help of BK. AM and BK implemented and performed experiments and evaluations. JB wrote the paper.

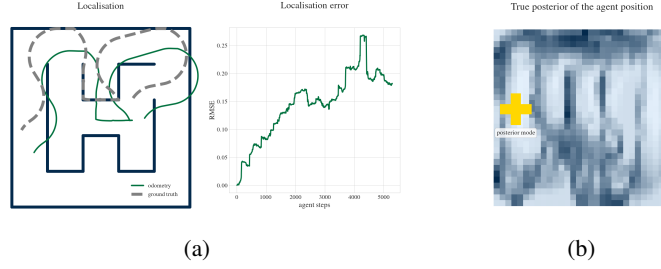


Figure 1: Examples of localisation. (a) Odometry-based. Left: 300 time steps at the end of the sequence where the solution has already drifted away from the ground truth. Right: Complete localisation error over a whole trajectory. (b) Plot of the posterior over the locations given the observation. It is highly non-Gaussian and has several maxima.

many SLAM approaches (e.g. Montemerlo et al. (2002); Paz et al. (2008); Grisetti et al. (2010)) but is limiting in practice: it is only tractable in a few basic cases such as linear Gaussian systems. Consequently, state of the art applications of SLAM (Mur-Artal et al., 2015) induce assumptions due to reasons of computational tractability rather than probabilistic model validity.

Several works were proposed recently that overcome the intractabilities of Bayes filters via approximate inference. Higher flexibility comes at the cost of only obtaining an approximate solution; yet these approaches often achieve outstanding results (Gu et al., 2015; Krishnan et al., 2015; Karl et al., 2016; Fraccaro et al., 2016; Maddison et al., 2017). Typically, the optimisation of finding an approximate posterior is amortised into a fixed computation implemented as a neural network; this approach is hence often referred to as amortised inference (Rezende et al., 2014; Kingma and Welling, 2014).

Our contribution is the application of such variational Bayes filters to the SLAM problem. A central challenge is the complex shape of the posterior over the pose given the current observation (cf. fig. 1): its shape is highly non-Gaussian and reflects the characteristics of the current belief of the environment.

To facilitate research, we propose a simulator that lets a holonomic agent equipped with laser range finders traverse simple square mazes. We augment a variational Bayes filter with a global latent variable representing the map, which is integrated into the emission model through an attention mechanism controlled by the current pose. Two major challenges—that of training a single, long, consecutive time series and that of complex posteriors—are overcome through a heuristic, particle-based scheme and an importance-sampling-based approximation. The resulting method outperforms a motion-model-based baseline in terms of localisation, learns realistic map representations and provides the user with a fully probabilistic model.

## 2 Methods

Consider a probabilistic graphical model of the form

$$p(\mathbf{x}_{1:T}, \mathbf{z}_{1:T}, \mathbf{m}_{1:T}, \mathcal{M} \mid \mathbf{u}_{1:T-1}) = p(\mathcal{M}) \rho(\mathbf{z}_1) \prod_{t=1}^T p(\mathbf{x}_t \mid \mathbf{m}_t) p(\mathbf{m}_t \mid \mathbf{z}_t, \mathcal{M}) \prod_{t=1}^{T-1} p(\mathbf{z}_{t+1} \mid \mathbf{z}_t, \mathbf{m}_t, \mathbf{u}_t), \quad (1)$$

where  $\mathbf{x}_{1:T} \in \mathbb{R}^{T \times D_x}$  is a sequence of observations,  $\mathbf{z}_{1:T} \in \mathbb{R}^{T \times D_z}$  is a sequence of poses,  $\mathbf{m}_{1:T} \in \mathbb{R}^{T \times D_m}$  is a sequence of charts and  $\mathbf{u}_{1:T-1} \in \mathbb{R}^{(T-1) \times D_u}$  is a sequence of control inputs. Let  $\mathcal{M}$  be a global random variable, the *map*, which relates the current pose  $\mathbf{z}_t$ , successor pose  $\mathbf{z}_{t+1}$  and observation  $\mathbf{x}_t$  through a local chart  $\mathbf{m}_t$  at each time step. Intuitively, the chart is the region of the map that is currently relevant.

The model constitutes a latent Markov model, which can be seen if both the map  $\mathcal{M}$  and the local charts  $\mathbf{m}_{1:T}$  are marginalised out. This model is commonly used in robotic navigation tasks (e.g. (Montemerlo et al., 2002)). It is depicted in fig. 3.

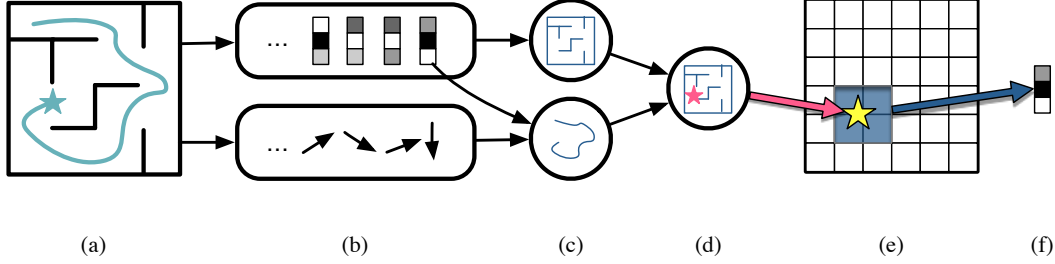


Figure 2: Illustration of the computation. The use of neural networks and attention mechanisms renders the whole pipeline differentiable and gradient-based optimisation can thus be applied. (a) An agent depicted as a teal star is traversing a maze. (b) Two data streams are generated, the sensor readings (top) and the taken control signals (bottom). (c) A first belief of the pose is formed based on the observations only, making use of an internal map (top). Another belief is formed based on the transition model, i.e. the taken control signals and intermediate information from the observation. (d) Sensor fusion is applied to the two beliefs to obtain a joint belief over the pose. (e) The pose is used to index a map with an attention mechanism. (f) The attended region of the map is used to reconstruct the observation, necessary for learning.

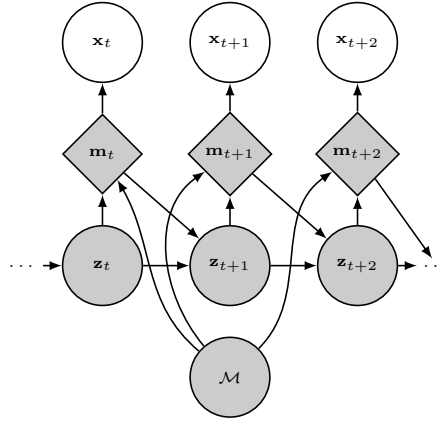


Figure 3: The probabilistic graphical model used in this work, except for parameters  $\theta$ .

A common assumption is that the factors are governed by a set of parameters  $\theta$ , i.e.  $\rho_{\theta_t}(\mathbf{z}_1)$ ,  $p_{\theta_T}(\mathbf{z}_{t+1} \mid \mathbf{z}_t, \mathbf{u}_t, \mathbf{m}_t)$ ,  $p_{\theta_E}(\mathbf{x}_t \mid \mathbf{m}_t)$ . We will leave out the dependency for notational brevity in the remainder of this work. Further, we will assume that the transition model and the initial state distribution are known or learned *a priori*.

## 2.1 Approximation via variational inference

Inference in models such as eq. (1) is intractable in most cases. We will use the approach described by Karl et al. (2016) for inference of the map  $\mathcal{M}$  and the poses  $\mathbf{z}_{1:T}$ . The parameters  $\theta$  are assumed to be known. We use variational distributions, i.e.  $q(\mathcal{M})$  and  $q(\mathbf{z}_{1:T} \mid \mathbf{x}_{1:T}, \mathbf{u}_{1:T-1})$ , where we rely on Bayes by backprop (Blundell et al., 2015) for the former and on SGVB (Kingma and Welling, 2014) for the latter. Given a sequence of observations  $\mathbf{x}_{1:T}$  and a sequence of control signals  $\mathbf{u}_{1:T-1}$ , a variational upper bound on the negative log-likelihood of the data is optimised. The negative *evidence*

lower bound (ELBO) is given as

$$\begin{aligned} \mathcal{L}_{\text{elbo}} = & \underbrace{\mathbb{E} [-\log p(\mathbf{x}_{1:T} | \mathbf{z}_{1:T}, \mathcal{M}, \mathbf{u}_{1:T-1})]}_{=:\ell^r} + \\ & \underbrace{\text{KL}[q(\mathbf{z}_{1:T} | \mathbf{x}_{1:T}, \mathbf{u}_{1:T-1}, \mathcal{M}) || p(\mathbf{z}_{1:T} | \mathbf{u}_{1:T-1}, \mathcal{M})]}_{=:\ell^z} + \\ & \underbrace{\text{KL}[q(\mathcal{M}) || p(\mathcal{M})]}_{=:\mathcal{L}^{\mathcal{M}}}, \end{aligned} \quad (2)$$

where the expectation is with respect to the variational distributions  $\mathcal{M} \sim q(\mathcal{M})$  and  $\mathbf{z}_{1:T} \sim q(\mathbf{z}_{1:T} | \mathbf{x}_{1:T}, \mathbf{u}_{1:T-1})$ . We call  $\ell^r$  the *reconstruction loss*,  $\ell^z$  the *pose KL penalty* and  $\mathcal{L}^{\mathcal{M}}$  the *map KL penalty*. Each  $q$  will be indexed by a set of variational parameters, which we collect in  $\phi$ . Inference of poses and the map then comes down to the minimisation of eq. (2) with respect to  $\phi$ . The interested reader is referred to Karl et al. (2016) for an elaborate discussion on the design of the amortised inference model  $q(\mathbf{z}_{1:T} | \mathbf{x}_{1:T}, \mathbf{u}_{1:T-1})$ .

## 2.2 Implementation of the generative model

Following Murphy (1999), we define the map  $\mathcal{M}$  to be a finite grid of width  $w$  and height  $h$ . Each grid cell  $\mathcal{M}_{ij}$  is a real-valued vector of dimensionality  $D_m$ , i.e.  $\mathcal{M} \in \mathbb{R}^{w \times h \times D_m}$ . As prior of such a latent map cell we use a standard normal,  $\mathcal{M}_{ij} \sim \mathcal{N}(\mathbf{0}, \mathbf{1})$ . Extracting *local charts*  $\mathbf{m}_t$  from the map is done through a convex combination of all memory cells:

$$\mathbf{m}_t = f_m(\mathcal{M}, \mathbf{z}_t) = \sum_{i,j} \alpha(\mathbf{z}_t)_{ij} \mathcal{M}_{ij}, \quad \text{s.t.} \quad \sum_{i,j} \alpha(\mathbf{z}_t)_{ij} = 1,$$

as usually done in attention models (Bahdanau et al., 2014). The result is then a point mass:  $p(\mathbf{m}_t | \mathbf{z}_t, \mathcal{M}, \theta_M) \propto \mathbb{I}[\mathbf{m}_t = f_m(\mathbf{z}_t, \mathcal{M})]$ . In this implementation, we consider  $\alpha$  to be a bilinear kernel.

The *emission model* or likelihood is represented through a homoskedastic conditional Gaussian distribution. The mean is given by a neural network  $\mu_E$  which is parameterised by  $\theta_E$ , i.e.

$$p(\mathbf{x}_t | \mathbf{m}_t) = \mathcal{N}(\mu_E(\mathbf{m}_t), \text{diag}(\sigma_E^2)).$$

The variance  $\sigma_E^2$  is specified component-wise and also included in the parameters  $\theta_E$ .

For the *transition model* we use a homoskedastic conditional Gaussian distribution as well; its mean is a function of the current pose, control signal and chart, which we represent as a neural network  $\mu_T$  parameterised by  $\theta_T$ :

$$p(\mathbf{z}_{t+1} | \mathbf{z}_t, \mathbf{u}_t, \mathbf{m}_t) = \mathcal{N}(\mu_T(\mathbf{z}_t, \mathbf{u}_t, \mathbf{m}_t), \sigma_T^2 \mathbf{1}).$$

The dependence on the current chart allows the transition to account for collisions at its current location. The variance  $\sigma_T^2$  is part of the parameters  $\theta_T$ .

## 2.3 Design of the variational posterior

Inference of poses is done through a variational approximation of the true posterior  $q(\mathbf{z}_t | \mathbf{x}_{1:T}) \approx p(\mathbf{z}_t | \mathbf{x}_{1:T})$ , where we left out the control signals  $\mathbf{u}_{1:T-1}$  for brevity and will do so for the remainder of this section. The global variable  $\mathcal{M}$  poses an atypical challenge for stochastic recurrent models trained with amortised variational inference, for which an intuitive explanation is as follows. Consider the true posterior, which has to account for all possible maps:

$$p(\mathbf{z}_t | \mathbf{x}_{1:T}) = \int p(\mathbf{z}_t | \mathcal{M}, \mathbf{x}_{1:T}) p(\mathcal{M} | \mathbf{x}_{1:T}) d\mathcal{M}.$$

Any parameterised variational approximation  $q(\mathbf{z}_t | \mathbf{x}_{1:T})$  will have to implement its own belief of the map implicitly. During training, this will prove difficult as it has to track the current belief of the generative model to conform to it, as it essentially implements its inverse (cf. fig. 1). The task of the inference model can be substantially eased by informing it of the current belief of the map  $q(\mathcal{M})$

explicitly. We do so by implementing  $q$  as a particle filter with the particle forwarding distribution from section 2.4.3 as a proposal distribution:

$$\begin{aligned} q(\mathbf{z}_t \mid \mathbf{x}_{1:t}, \mathcal{M}) &\propto \mathbb{E}_{\mathbf{z}_t^{(k)} \sim \hat{q}(\mathbf{z}_t)} \left[ \sum_{k=1}^K \hat{\omega}_k \right], \\ \hat{\omega}_k &= \frac{\omega_k}{\sum_j \omega_j}, \\ \omega_k &= \frac{p(\mathbf{x}_t \mid \mathbf{z}_t^{(k)}, \mathcal{M}) p(\mathbf{z}_t^{(k)})}{\hat{q}(\mathbf{z}_t^{(k)})}, \end{aligned}$$

This has two immediate consequences. First, the variational posterior used does not have any parameters and is hence not optimised directly. Second, the true posterior is recovered for  $K \rightarrow \infty$ . But most importantly, the importance weights explicitly reflect the map (sampled from an outer expectation over  $q(\mathcal{M})$ ) and the proposals in conflict with it will be sorted out in a natural manner as they have lower weights.

The variational approximation of the posterior map  $q(\mathcal{M})$  was chosen to follow a mean-field approach with a factorized Gaussian  $q(\mathcal{M}) = \prod_i \prod_j \mathcal{N}(\boldsymbol{\mu}_{\mathcal{M}_{ij}}, \boldsymbol{\sigma}_{\mathcal{M}_{ij}}^2)$ , with variational parameters  $\boldsymbol{\mu}_{\mathcal{M}_{ij}}, \boldsymbol{\sigma}_{\mathcal{M}_{ij}}^2 \in \phi$ .

## 2.4 Faster training with mini batches

The objective function eq. (2) is problematic since it is not obvious how to exploit parallel architectures such as GPUs to their full extent: we show in section 2.4.1 that it consists of  $T$  terms, one for each time step. Each depends at least on its immediate predecessor through the transition probability and optionally the variational approximation. To propose a heuristic approach that allows parallel computation of those terms, we revisit stochastic gradient descent (Bottou, 1991) in section 2.4.2. Our approach, presented in section 2.4.3, approximates the gradient at each time step without having to sample the whole latent pose trajectory. This comes, however, at the cost of biased gradients.

### 2.4.1 Decomposing the loss into a sum over time steps

Under the Markov assumptions, the evidence lower bound can be written as a sum over time steps. For the reconstruction loss, we have

$$\ell^r = \mathbb{E}_{\mathbf{z}_{1:T} \sim q} [-\log p(\mathbf{x}_{1:T} \mid \mathbf{z}_{1:T})] = \sum_{t=1}^T \underbrace{\mathbb{E}_{\mathbf{z}_t \sim q} [-\log p(\mathbf{x}_t \mid \mathbf{z}_t)]}_{=: \ell_t^r},$$

and for the pose KL penalty

$$\ell^z = \mathbb{E}_{\mathbf{z}_{1:T} \sim q} \left[ -\log \frac{q(\mathbf{z}_{1:T})}{p(\mathbf{z}_{1:T})} \right] = \sum_{t=1}^T \underbrace{\mathbb{E}_{\mathbf{z}_t, \mathbf{z}_{t-1} \sim q} \left[ -\log \frac{q(\mathbf{z}_t)}{p(\mathbf{z}_t \mid \mathbf{z}_{t-1})} \right]}_{=: \ell_t^z},$$

where we have left out the condition of  $q(\mathbf{z}_t)$  and the control signals  $\mathbf{u}_{1:T-1}$  for brevity. The map KL penalty is not part of the sum, but as shown in Blundell et al. (2015) it is possible to distribute its contribution over different time steps. We do so uniformly, i.e. we write it as a sum of  $T$  terms, each weighed equally:  $\mathcal{L}^{\mathcal{M}} = \sum_{t=1}^T \frac{1}{T} \ell^{\mathcal{M}}$ . Hence,

$$\mathcal{L}_{\text{elbo}} = \mathbb{E}_{\mathbf{z}_{1:T} \sim q} \left[ \sum_{t=1}^T \ell_t^r + \ell_t^z + \ell^{\mathcal{M}} \right]. \quad (3)$$

We denote the overall loss at time step  $t$  as  $\mathcal{L}_t$ .

### 2.4.2 Stochastic gradient descent

Stochastic gradient descent is based on the insight that for convergence only an unbiased estimate of the gradient is necessary (Bottou, 1991). Formally, at iteration  $i$  we perform the update<sup>1</sup>

$$\phi^{(i+1)} \leftarrow \phi^{(i)} + \eta^{(i)} \tilde{\nabla}_{\phi}^{(i)},$$

where  $\eta^{(i)}$  is a component-wise learning rate,  $\phi^{(i)}$  are the parameters of interest and  $\tilde{\nabla}_{\phi}^{(i)}$  is an estimate of the gradient of the loss function with respect to  $\phi$ . This method will converge to an optimum under mild assumptions on the learning rates and if

$$\mathbb{E} [\tilde{\nabla}_{\phi}] = \frac{\partial \mathcal{L}}{\partial \phi},$$

i.e.  $\tilde{\nabla}_{\phi}$  is an unbiased estimator of the gradient. A popular estimator is to use mini batches, sometimes referred to as data subsampling: as the loss function is a sum over independent terms, using only a subset of them to estimate the gradient will result in an unbiased estimator of the gradient. As we have shown in eq. (3), our objective can indeed be represented in this fashion. Unfortunately, it is an expectation over elements of the pose trajectory, which requires sampling from the whole Markov chain via ancestral sampling.

### 2.4.3 Approximate Asynchronous Particle Representation

Alleviation of this computational difficulty is done through approximate data subsampling: we maintain a set of particles  $\xi_t^{(n)}$ ,  $n = 1, \dots, N$ ;  $t = 1, \dots, T$  that cache samples from the variational posterior over the poses over training iterations. These particles are updated only occasionally—every time the corresponding time step is used to estimate gradients. Note that these particles are different from the samples used to estimate eq. (2). A detailed description of the procedure is as follows.

The time steps we wish to use for gradient estimation are gathered in a minibatch  $\mathcal{B}$ , all other time steps are contained in  $\bar{\mathcal{B}}$ . We then approximate the loss given in eq. (3) via

$$\tilde{\mathcal{L}} = \mathbb{E}_{\mathbf{z}_{1:T} \sim \hat{q}} \left[ \sum_{t \in \mathcal{B}} \ell_t^r + \ell_t^z + \ell^{\mathcal{M}} \right], \quad (4)$$

where  $\hat{q}$  is an approximation of  $q$  that allows more efficient sampling of  $\mathbf{z}_t$ . In this work,  $\hat{q}$  is represented as a Normal random variable with moments matched from a set of  $N$  particles:

$$\hat{q}(\mathbf{z}_t) = \mathcal{N}(\mu_{\xi_t}, \sigma_{\xi_t}^2),$$

where  $\mu_{\xi_t} = \frac{1}{N} \sum_{n=1}^N \xi_t^{(n)}$  and  $\sigma_{\xi_t}^2 = \frac{1}{N} \sum_{n=1}^N (\mu_{\xi_t} - \xi_t^{(n)})^2$  are the empirical mean and variance of the particles respectively. The particles at time step  $t$  are obtained during the estimation of the gradients: for any training iteration with  $t \in \mathcal{B}$ , we can update the particles at the following time steps  $t \in \bar{\mathcal{B}}$ :

$$\xi_{t+K}^{(n)} \sim q(\mathbf{z}_t) \prod_{k=1}^K p(\mathbf{z}_{t+k} | \mathbf{z}_{t+k-1}).$$

This essentially leads to an asynchronous procedure: expectations are implemented through particles stemming from previous training iterations, potentially biasing the gradients further. This bias can be controlled with small updates (i.e.  $\phi^{(i+1)} \approx \phi^{(i)}$ ), since we can then expect the expectations to be close as well. A convenient schedule is to pick minibatches that consist of consecutive time steps. In this work, we slice the training sequences into chunks of equal length  $K$  and form a minibatch to consist of a fixed number of such slices.

## 3 Related Work

The problem of concurrent estimation of an agent’s pose and its surrounding has seen considerable attention in the last decades. We refer the interested reader to the survey of Cadena et al. (2016),

<sup>1</sup>Note that this holds for  $\theta$  instead of  $\phi$  as well.

which contains a thorough review of the relevant publications and methods; we will focus on those which are directly related to our work. We consider a contribution of Murphy (1999) most similar to our approach: the treatment of the map as a matrix-valued global latent variable which is inferred through approximate Bayesian methods. Our work brings a range of modern techniques to the table, which have been pioneered in different works over the recent years. The use of neural network based architectures appears obvious, also since it has been shown that SLAM can be performed implicitly in a recurrent neural network (Kanitscheider and Fiete, 2017).

Mapping and localisation has been adopted in the machine-learning community mostly to solve reinforcement-learning or visual-navigation problems where the model is often tightly integrated with the inference method. Bhatti et al. (2016) integrated an engineered pipeline into an agent for learning to play the computer game Doom. Oh et al. (2016) took a different approach by equipping an agent with an external memory which is not informed about the spatial structure of its environment. This prior knowledge was then added to the architecture of the agent’s policy by Parisotto and Salakhutdinov (2017). To the same end Fraccaro et al. (2018) integrated this prior into the model for model-based reinforcement learning. While their approach is similar to ours their focus was primarily on simulator performance over long time spans. Further, an external memory is used which does not directly represent a random variable as part of a graphical model. Gupta et al. (2017) integrated their planning within a mapping framework. Interestingly, Savinov et al. (2018) reduced visual navigation to a few supervised learning components; they explicitly side-stepped the task of metric localisation. Zhu et al. (2017) also performed visual navigation via deep reinforcement learning but explicitly left out mapping the environment. Parisotto et al. (2018) used a neural architecture for localisation; a graph of observations can be seen as a map, which is then used to iteratively refine a pose trajectory.

Since amortised variational inference (Kingma and Welling, 2014; Rezende et al., 2014) was applied to recurrent networks (Bayer and Osendorfer, 2014), sequential latent variable models based on neural architectures have seen progress at multiple ends. Chung et al. (2015); Johnson et al. (2016) applied more sophisticated architectures of inference models. State-space models were also considered here, and focussed upon by others (Krishnan et al., 2015; Karl et al., 2016; Fraccaro et al., 2016). Watter et al. (2015) applied ideas of amortised variational inference to the setting of Markov decision processes, but a proper generative and recurrent model in this context was not proposed until (Karl et al., 2016). Particle filter-based schemes were used previously by Gu et al. (2015); Maddison et al. (2017). Adding external memory components to such models was studied by Gemici et al. (2017).

## 4 Experiments

The aim of the experiments was to test whether the proposed approximation of the graphical model outperforms a baseline based on the transition  $p(\mathbf{z}_{t+1} | \mathbf{z}_t, \mathbf{u}_t, \mathbf{m}_t)$  only. No other base lines from the literature were considered as these are either not a generative model or not fully differentiable. We used a precisely controlled environment, and hence implemented our own simulator using pybox2d<sup>2</sup>. A detailed description can be found in appendix A. For data collection, we randomised seven distinct mazes. Each was traversed by two human operators, resulting in 6 trajectories per maze of length 3000 steps each. The transition model  $p(\mathbf{z}_{t+1} | \mathbf{z}_t, \mathbf{u}_t, \mathbf{m}_t)$  was pretrained on a first maze that was not considered during evaluation. For this, the true poses were used for approximately 20’000 steps. The initial pose  $\mathbf{z}_1$  was assumed to be  $\mathbf{0}$  without loss of generality, making learning the initial distribution  $\rho(\mathbf{z}_1)$  unnecessary. Performing SLAM then consisted of approximating the posterior of the poses and the map  $p(\mathbf{z}_{1:t}, \mathcal{M} | \mathbf{x}_{1:t}, \mathbf{u}_{1:t-1})$  through the optimisation of eq. (2) with respect to the variational posteriors  $q(\mathbf{z}_{1:T})$  and  $q(\mathcal{M})$ . The optimisation was conducted with stochastic gradient descent using ADAM Kingma and Ba (2014). The observation sequence was partitioned into slices of length 10 and the approximate scheme introduced in section 2.4.3 was used. Details on the model architectures can be found in appendix B.

We considered two cases, *offline* and *online SLAM*. In the first case, we used  $t = T$  to obtain  $q(\mathbf{z}_{1:T})$ , while we swept  $t = 1, \dots, T$  in the second case to obtain time-step-wise estimates  $q(\mathbf{z}_t)$ .

**Evaluation of localisation performance** The final pose estimation for calculation of the localisation error consisted of an average of the particles via  $\tilde{\omega}_i = \frac{\exp(\tilde{\omega}_i/10)}{\sum_j \exp(\tilde{\omega}_j/10)}$  to obtain stable results. For

<sup>2</sup><https://github.com/pybox2d/pybox2d>

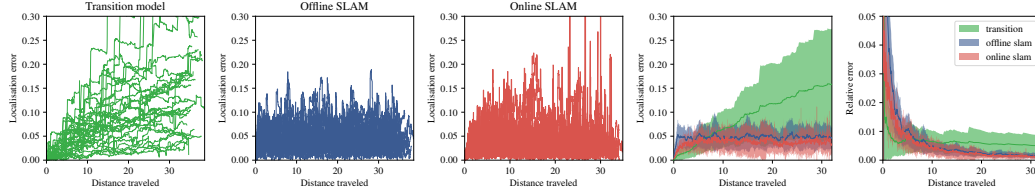


Figure 4: We show the individual estimates of rollouts on the validation mazes for transition model, offline and online SLAM in the first three plots from the right. The fourth plot shows the aggregate results with confidence intervals. The last plot shows the localisation error relative to the distance travelled. The transition model quickly drifts away from the right solution. Both SLAM approaches are able to correct the drift; notably, offline SLAM performs slightly worse but more robustly than online SLAM.

offline SLAM, the final variational approximations were used. For online SLAM, the variational approximations found after the respective iteration  $t$  were used.

**Quantitative results** For both online and offline SLAM, using a map clearly outperforms the base line using only the motion model:  $0.03 \pm 0.02$  and  $0.04 \pm 0.02$  at time step 3000 for online and offline SLAM respectively. At this time step, the motion model has practically diverged for most of the sequences with an average error of  $0.14 \pm 0.1$ , even though the model was trained on approx. 20'000 transitions. Most notably, the use of a map practically eliminates drift: after 3000 steps, a relative error of less than  $20000^{-1}$ , practically zero, is obtained. This shows that our method stabilises the motion model and keeps the location estimate from diverging. We illustrate the findings in fig. 4.

**Qualitative results** To assess the quality of the estimated map, we investigated our model further. To verify whether the architecture of the maze, i.e. its walls, are correctly captured by the map and the emission model, we placed the agent at random in the maze and drew from the corresponding emission model, i.e. sampling from  $p(\mathbf{x}, \mathbf{z})$ . The resulting emission represents the distance reading of 20 laser range finders, which we convert into a scatter plot as such. Each point is the end of a line segment starting out at the agent's location going into the direction of one of the laser range finders. The length of the line segment is exactly that of the respective emission component. Hence we plot the points where the model believes the laser range finders to hit a wall. The resulting plots are shown in fig. 5 (a)-(c); videos of the development through the course of online SLAM can be found in the supplementary material.

## 5 Discussions and Conclusion

We have introduced a variational Bayes filter that integrates a global latent variable of a spatial form. By carefully choosing the transition distribution, posterior inference can be related to solving the problem of simultaneous localisation and mapping. The novelty of our contribution lies in the flexibility that is inherited from neural networks and variational inference: contrary to most recent work in the area, our model still constitutes a generative model, which allows types of inference which go beyond this work. Still, the method complies with the de facto standard formulation of SLAM. For experimental evaluation, we designed and implemented a seemingly simple environment which exhibits several challenges, such as multimodal posteriors. Overcoming these challenges required us to devise a special design of inference models and a heuristic learning for very long sequences. The experimental results show a clear improvement over an accurate motion model, bearing promise for real-world application.

**Author contributions** PvdS and JB conceived the project. JB lead the project. AM, BK and JB devised the method. AM implemented the method with help of BK. AM and BK implemented and performed experiments and evaluations. JB wrote the paper.



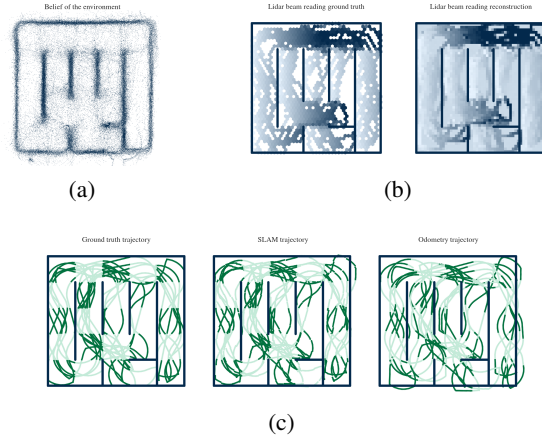


Figure 5: Qualitative results obtained from SLAM on one of the six validation mazes. (a) Scatter plot of observations, used to visualise the map. We sample from the joint  $p(\mathbf{z}, \mathbf{x})$ . For each of the 20 emission components, we move along the direction of the corresponding laser beam for the sampled value of the laser range finder and plot a point there. The plot clearly resembles the architecture of the maze. (b) The value of the laser range finder heading west according to the empirical distribution on the left and according to the model on the right. (c) Filtering of the trajectory, showing the true trajectory on the left, the one inferred via SLAM in the middle and the one based on the motion model only on the right.

## References

- Bahdanau, D., Cho, K., and Bengio, Y. (2014). Neural machine translation by jointly learning to align and translate. *CoRR*, abs/1409.0473.
- Bayer, J. and Osendorfer, C. (2014). Learning stochastic recurrent networks. *CoRR*, abs/1411.7610.
- Bhatti, S., Desmaison, A., Miksik, O., Nardelli, N., Siddharth, N., and Torr, P. H. S. (2016). Playing doom with slam-augmented deep reinforcement learning. *CoRR*, abs/1612.00380.
- Blundell, C., Cornebise, J., Kavukcuoglu, K., and Wierstra, D. (2015). Weight uncertainty in neural networks. *CoRR*, abs/1505.05424.
- Bottou, L. (1991). Stochastic gradient learning in neural networks. In *Proceedings of Neuro-Nîmes 91*, Nîmes, France. EC2.
- Cadena, C., Carlone, L., Carrillo, H., Latif, Y., Scaramuzza, D., Neira, J., Reid, I. D., and Leonard, J. J. (2016). Past, present, and future of simultaneous localization and mapping: Toward the robust-perception age. *IEEE Trans. Robotics*, 32(6):1309–1332.
- Chung, J., Kastner, K., Dinh, L., Goel, K., Courville, A. C., and Bengio, Y. (2015). A recurrent latent variable model for sequential data. In *Advances in Neural Information Processing Systems 28: Annual Conference on Neural Information Processing Systems 2015, December 7-12, 2015, Montreal, Quebec, Canada*, pages 2980–2988.
- Fraccaro, M., Rezende, D. J., Zwols, Y., Pritzel, A., Eslami, S. M. A., and Viola, F. (2018). Generative temporal models with spatial memory for partially observed environments. *CoRR*, abs/1804.09401.
- Fraccaro, M., Sønderby, S. K., Paquet, U., and Winther, O. (2016). Sequential neural models with stochastic layers. In *Advances in Neural Information Processing Systems 29: Annual Conference on Neural Information Processing Systems 2016, December 5-10, 2016, Barcelona, Spain*, pages 2199–2207.
- Gemici, M., Hung, C., Santoro, A., Wayne, G., Mohamed, S., Rezende, D. J., Amos, D., and Lillicrap, T. P. (2017). Generative temporal models with memory. *CoRR*, abs/1702.04649.

- Grisetti, G., Kümmerle, R., Stachniss, C., and Burgard, W. (2010). A tutorial on graph-based SLAM. *IEEE Intell. Transport. Syst. Mag.*, 2(4):31–43.
- Gu, S., Ghahramani, Z., and Turner, R. E. (2015). Neural adaptive sequential monte carlo. In *Advances in Neural Information Processing Systems 28: Annual Conference on Neural Information Processing Systems 2015, December 7-12, 2015, Montreal, Quebec, Canada*, pages 2629–2637.
- Gupta, S., Davidson, J., Levine, S., Sukthankar, R., and Malik, J. (2017). Cognitive mapping and planning for visual navigation. In *2017 IEEE Conference on Computer Vision and Pattern Recognition, CVPR 2017, Honolulu, HI, USA, July 21-26, 2017*, pages 7272–7281.
- Johnson, M. J., Duvenaud, D. K., Wiltchko, A., Adams, R. P., and Datta, S. R. (2016). Composing graphical models with neural networks for structured representations and fast inference. In *Advances in Neural Information Processing Systems 29: Annual Conference on Neural Information Processing Systems 2016, December 5-10, 2016, Barcelona, Spain*, pages 2946–2954.
- Kanitscheider, I. and Fiete, I. (2017). Training recurrent networks to generate hypotheses about how the brain solves hard navigation problems. In *Advances in Neural Information Processing Systems 30: Annual Conference on Neural Information Processing Systems 2017, 4-9 December 2017, Long Beach, CA, USA*, pages 4532–4541.
- Karl, M., Sölch, M., Bayer, J., and van der Smagt, P. (2016). Deep variational bayes filters: Unsupervised learning of state space models from raw data. *CoRR*, abs/1605.06432.
- Kingma, D. and Welling, M. (2014). Auto-encoding variational bayes. In *Proceedings of the 2nd International Conference on Learning Representations (ICLR)*.
- Kingma, D. P. and Ba, J. (2014). Adam: A method for stochastic optimization. *CoRR*, abs/1412.6980.
- Krishnan, R. G., Shalit, U., and Sontag, D. (2015). Deep kalman filters. *CoRR*, abs/1511.05121.
- Maddison, C. J., Lawson, J., Tucker, G., Heess, N., Norouzi, M., Mnih, A., Doucet, A., and Teh, Y. W. (2017). Filtering variational objectives. In *Advances in Neural Information Processing Systems 30: Annual Conference on Neural Information Processing Systems 2017, 4-9 December 2017, Long Beach, CA, USA*, pages 6576–6586.
- Montemerlo, M., Thrun, S., Koller, D., and Wegbreit, B. (2002). Fastslam: A factored solution to the simultaneous localization and mapping problem. In *Proceedings of the Eighteenth National Conference on Artificial Intelligence and Fourteenth Conference on Innovative Applications of Artificial Intelligence, July 28 - August 1, 2002, Edmonton, Alberta, Canada.*, pages 593–598.
- Mur-Artal, R., Montiel, J. M. M., and Tardós, J. D. (2015). ORB-SLAM: A versatile and accurate monocular SLAM system. *IEEE Trans. Robotics*, 31(5):1147–1163.
- Murphy, K. P. (1999). Bayesian map learning in dynamic environments. In *Advances in Neural Information Processing Systems 12, [NIPS Conference, Denver, Colorado, USA, November 29 - December 4, 1999]*, pages 1015–1021.
- Oh, J., Chockalingam, V., Singh, S. P., and Lee, H. (2016). Control of memory, active perception, and action in minecraft. In *Proceedings of the 33rd International Conference on Machine Learning, ICML 2016, New York City, NY, USA, June 19-24, 2016*, pages 2790–2799.
- Parisotto, E., Chaplot, D. S., Zhang, J., and Salakhutdinov, R. (2018). Global pose estimation with an attention-based recurrent network. *CoRR*, abs/1802.06857.
- Parisotto, E. and Salakhutdinov, R. (2017). Neural map: Structured memory for deep reinforcement learning. *CoRR*, abs/1702.08360.
- Paz, L. M., Pinies, P., Tardós, J. D., and Neira, J. (2008). Large-scale 6-dof SLAM with stereo-in-hand. *IEEE Trans. Robotics*, 24(5):946–957.
- Rezende, D. J., Mohamed, S., and Wierstra, D. (2014). Stochastic backpropagation and approximate inference in deep generative models. In *Proceedings of the 31th International Conference on Machine Learning, ICML 2014, Beijing, China, 21-26 June 2014*, pages 1278–1286.

- Savinov, N., Dosovitskiy, A., and Koltun, V. (2018). Semi-parametric topological memory for navigation. *CoRR*, abs/1803.00653.
- Watter, M., Springenberg, J. T., Boedecker, J., and Riedmiller, M. A. (2015). Embed to control: A locally linear latent dynamics model for control from raw images. In *Advances in Neural Information Processing Systems 28: Annual Conference on Neural Information Processing Systems 2015, December 7-12, 2015, Montreal, Quebec, Canada*, pages 2746–2754.
- Zhu, Y., Mottaghi, R., Kolve, E., Lim, J. J., Gupta, A., Fei-Fei, L., and Farhadi, A. (2017). Target-driven visual navigation in indoor scenes using deep reinforcement learning. In *2017 IEEE International Conference on Robotics and Automation, ICRA 2017, Singapore, Singapore, May 29 - June 3, 2017*, pages 3357–3364.

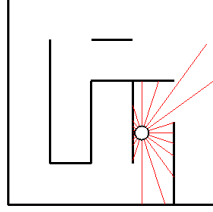


Figure 6: Illustration of the maze environment. The maze fills the unit square and is bounded by walls from all sides. The agent’s pose  $\mathbf{z}$  is its coordinates and rotation. The sensor readings are shown as lines emerging from the centre of the agent and go in all directions.

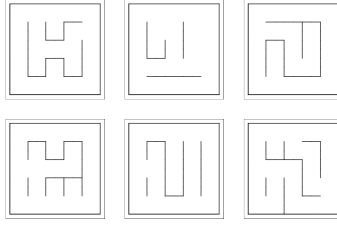


Figure 7: The six random mazes used for evaluation.

## A Physical simulator for mazes

In this environment, an agent traverses a single square maze of side length 1, which has been randomly generated. The agent is modeled as a dynamic body that can move in the specified maze environment. Its pose is specified by its coordinates in the maze’s plane  $\mathbf{p}_t \in \mathbb{R}^2$  and its orientation  $\alpha_t \in [-\pi, \pi]$ , which we collect in  $\mathbf{z}_t = (\mathbf{p}_t, \alpha_t)$ . We assume the agent has a radius of  $10^{-5}$ . Additionally, its restitution parameter, which normally controls the bouncing off of objects after collisions with other bodies, is set to 0. We define the agent’s sensor to be a range finder with 20 line segments covering a full circle surrounding the agent ( $\frac{2\pi}{20}$  angular difference between neighboring beams); its response is the Euclidean distance to an object intersecting with the ray. The length of each line segment is set to 0.53, and that value is also returned when there is no obstacle in a given beam’s reach. The agent’s movement is restricted by collisions with the maze walls. The agent is holonomic, as it can rotate freely with no obstruction, but can only move along the axis of its heading. The control signals specify rotational velocity  $\dot{\alpha}$  and a movement offset (directional derivative)  $\dot{\mathbf{p}}$ . In the simulator, first the rotational velocity is applied, followed by the movement offset.

## B Details of the model

### B.1 Emission model

- Input:  $\mathbf{m}_t$
- Output:  $\mathbf{x}_t$
- $\mu_E$  is realised via a feed-forward neural network with parameters  $\theta_E$  (cf. Table 1 for hyperparameters)

Table 1: Architectural details of the networks used to realise the emission and transition models.

model	# layers	# units	hidden activation	output	initialiser
emission, $\theta_E$	4	256	softsign	identity	Glorot uniform
transition, $\theta_T$	6	256	ReLU	identity	Glorot uniform

- The emission mean  $\mu_{\mathbf{x}_t}$  is formed by applying a rotational shift to the output of  $\mu_E(\mathbf{m}_t)$  w.r.t. the current estimate of the agent’s heading angle  $\phi_t = \mathbf{z}_t^{(1)}$ ; this is done to ensure the generalisation of charts  $\mathbf{m}_t$  for all different orientations of the agent
- The emission model’s standard deviation is globally set to 0.1:

$$\mathbf{x}_t = \mathcal{N}(\mu_{\mathbf{x}_t}, 0.1 \times \mathbf{I})$$

## B.2 Transition model

- Input:  $\mathbf{z}_t, \mathbf{u}_t, \mathbf{m}_t$
- Output:  $\mathbf{z}_{t+1}$
- $\mu_T$  is realised via a feed-forward neural network with parameters  $\theta_T$  (cf. Table 1 for hyperparameters)
- To avoid potential discontinuities in angular space, we transform  $\phi_t = \mathbf{z}_t^{(1)}$  (the agent’s heading at the current time step) to  $[\cos \phi_t, \sin \phi_t]^T$  before applying the transition model
- Instead of feeding  $\mathbf{m}_t$  into  $\mu_T$  directly, we choose to feed in  $\mu_E(\mathbf{m}_t)$  (the mean of the emission model, a deterministic transformation of  $\mathbf{m}_t$ ) — this allows us to pre-train the transition network using ground truth observations, as described in section 4.
- In our experiments, we assume no noise in the transition model, i.e.  $\sigma_T^2 \rightarrow 0$ .

## B.3 Memory

- $\mathcal{M} \in \mathbb{R}^{w \times h \times D_m}$ ,  $w = h = 32$ ,  $D_m = 10$
- Initialisation of the parameters of  $q(\mathcal{M})$  (inference):
$$\phi_{\mathcal{M}} = \{\mu_{\mathcal{M}_{ij}}, \sigma_{\mathcal{M}_{ij}}^2\}_{i \in [w], j \in [h]}, \mu_{\mathcal{M}_{ij}} = \mathbf{0}, \sigma_{\mathcal{M}_{ij}}^2 = \mathbf{1}$$

## B.4 Approximate Asynchronous Particle Representation

- Number of particles: 50
- Update frequency: particles are updated every 50 mini-batches, following the methodology layed out in section 2.4.3

## B.5 Optimization

- Optimizer: Adam,  $\beta_1 = 0.9$ ,  $\epsilon = 10^{-8}$
- Learning rate:  $10^{-4}$
- Batch-size: 128